Reliability of an offshore wind turbine with an uncertain S-N curve

Reliability of an offshore wind turbine with an uncertain S-N curve

Sebastian Drexler and Michael Muskulus

Norwegian University of Science and Technology NTNU
Department of Civil and Environmental Engineering

E-mail: sebastian.drexler@ntnu.no

Abstract. Probabilistic methods in wind turbine design are becoming more important in order to achieve a higher and more economic utilization of the structural resources. A design is thereby evaluated through its reliability by taking uncertainties into account. The influence of uncertainties emerging specifically within the fatigue limit state can be essential on a structure's reliability. For that reason, this study investigates two different sources for uncertainties within probabilistic fatigue design. The influence of a reduced approach, where the random behavior of a structural failure is only represented through an uncertain critical Miner sum, is compared to an approach, where also the S-N curve is subjected to uncertainties. For this, an offshore wind turbine with monopile support structure is investigated. The reliability analysis is performed through crude Monte Carlo simulations which utilize a Gaussian Process regression model in order to determine the wind turbine's structural response. The results show that both sources of uncertainties, the critical Miner sum and the S-N curve, contribute differently to the overall reliability. Uncertainties of the critical Miner sum have a rather small influence, whereas the implementation of an uncertain S-N curve leads to a noticeable increase of the reliability.

1. Introduction

1.1. Motivation

Wind turbine structures are well established electricity generators, for which a share in the global energy generation of approximately 15% is predicted for the year 2050 [1]. This will turn wind turbines into mass-produced articles with high expectations towards their profitability, and consequently their reliability. To fulfill these expectations from a structural perspective, the designs must be utilized efficiently. Current design standards require the application of semi-probabilistic approaches, which cover for uncertainties by application of partial safety factors. Since these are not custom-tailored to the structure under consideration, certain reserves may be still available, which can be detected and utilized. One promising approach is the analysis and prediction of a structure's reliability through fully probabilistic methods. Here, major uncertainties are considered during the design process. The structure is then designed for an adequate survival probability, or reliability. Since wind turbines are mainly exposed to dynamic loads, the fatigue strength is often the primary driver for the structural design. Consequently, investigating the structural reliability with focus on fatigue is of high interest. However, this can be challenging. For one thing, compared to a deterministic approach, the structural analysis within a reliability setting will now have to cover for a broad spectrum of configurations. This makes the already computationally elaborate fatigue investigation even more costly. For another thing, the overall effort will further increase with raising number of considered uncertainties. And these can be quite numerous within the design of wind turbines [2]. Naturally, in order to

maintain a certain performance or even to make a reliability estimation possible, one tries to reduce the quantity of considered uncertainties, e.g. by selecting only those, which are assumed to be most influential. This is sometimes the case in the fatigue post-processing part, where the Miner-Sum D is compared to a critical Miner-Sum D_{cr} in order to obtain a possible failure. Both variables possess uncertainties which should be considered during a reliability analysis based on the recommendations of the Joint Committee of Structural Safety (JCSS) [3]. The critical Miner-Sum D_{cr} is inherently uncertain and the Miner-Sum D is highly dependent on the structural response and the used S-N curve, which in turn, is based on material tests with distinct uncertainties. In some investigations, uncertainty in the fatigue post-processing is solely implemented by taking the variation of the critical Miner-Sum D_{cr} into account. The motivation for this investigation is therefore to detect the influence of this reduction on the reliability of a wind turbine's support structure, compared to the full post-processing approach.

1.2. Challenges

The implementation of a structural reliability approach which allows for a fatigue evaluation within an acceptable time frame is the most critical aspect within this investigation. For the verification of modern wind turbines several thousand load cases must be observed for a single fatigue analysis. In reliability investigations, where sampling methods are common, simulation time raises drastically since several fatigue analyses are required in order to achieve adequate accuracy.

1.3. Intention and Scope

We aim to demonstrate, how the reliability of a wind turbine is influenced by different fatigue strength verification approaches and how such verification routines can be implemented with computationally affordable methods. This is done based on a case study where a reference offshore wind turbine is implemented into a modern simulation environment and evaluated at a number of locations along its support structure.

2. Methods

2.1. Structural Reliability

The basic structural reliability approach incorporates the consideration of uncertainties into the structural design process. It provides information about the exceedance of certain design limits under defined conditions during a reference period in terms of estimates of their probabilities of occurrence [4]. Within the structural design process, the design limits leading to failure are usually of prime importance and used to determine the actual structural reliability, which is the probability to meet the design requirements, or in other words to maintain structurally safety without failure. The terms structural reliability $\mathfrak{R}$ and failure probability p_f are used equally to evaluate the structural performance of a design. They are commonly linked as

$$\mathfrak{R}\left(\boldsymbol{X}\right) = 1 - p_f. \tag{1}$$

To determine the necessary failure probability p_f, it is common to establish performance functions $G\left(\boldsymbol{X}\right)$. These relate the input uncertainties, which are therein described as random variables $\boldsymbol{X}$, with each other [5]. In the structural design process this is often illustrated with the basic reliability problem, or $R - S$ problem, where the performance function $G(R, S)$ is formed by one load effect S compared to one resistance R [6].

$$G(R, S) = R - S \tag{2}$$

The limit state function (LSF) $G(R, S) = 0$ divides the space of the random variables into a safe domain without failure ($G > 0$), and into a failure domain where the design requirements

are not met ($G < 0$). The probability of failure p_f is then equivalent to the probability that the basic random variables, in case of the basic reliability problem the load effect S and the resistance R, lie within the failure domain or directly on the LSF.

$$p_f = P\left[G(R,S) \leq 0\right] \tag{3}$$

Likewise, the reliability $\mathfrak{R}$ corresponds to the probability that these basic random variables are located within the remaining safe domain.

$$\mathfrak{R} = P\left[G(R,S) > 0\right] \tag{4}$$

For a general performance function $G\left(\boldsymbol{X}\right)$, the probability of failure p_f is calculated through the joint probability density function $f_{\boldsymbol{X}}\left(\boldsymbol{x}\right)$ considering all basic random variables $\boldsymbol{X}$ [6]. This leads to a multi-dimensional integration over the failure domain of the joint probability function. The number of integration dimensions corresponds to the number of basic random variables.

$$p_f = P\left[G(\boldsymbol{X}) \leq 0\right] = \int \cdots \int_{G(\boldsymbol{X})\leq 0} f_{\boldsymbol{X}}\left(\boldsymbol{x}\right) d\boldsymbol{x} \tag{5}$$

It is common to express the structural reliability not in terms of probabilities, but rather to set it in perspective to the standard normal distribution by using the so called reliability index β which is obtained from the standard normal inverse cumulative distribution function $\Phi^{-1}(x)$ [5].

$$\beta = \Phi^{-1}(\mathfrak{R}) = \Phi^{-1}(1 - p_f) \tag{6}$$

The reliability index β expresses the reliability $\mathfrak{R}$ as multiples of standard deviation from the mean. If, for example, two reliabilities $\mathfrak{R}_1 = 99.865\%$ and $\mathfrak{R}_2 = 99.999\%$ are compared, then the impression arises that their values are close together. However, an evaluation based on their reliability indices $\beta_1(\mathfrak{R}_1) = 3$ and $\beta_2(\mathfrak{R}_2) = 6$ helps to get a better impression, namely that these reliabilities are not close.

2.2. Monte Carlo Simulations

In order to solve equation 5 several different approaches exist, from direct and numerical integration, through simulation techniques to first- and second-order reliability methods [6]. A widely used approach in reliability analyses are Monte-Carlo simulation methods (MCS) since they are comparatively easy to implement, even for complex systems [7]. The MCS is a sampling method where every basic random variable X_i gets sampled, meaning a random number, determined as sample $\hat{x}_i$, is generated according to the basic variable's probability distribution $f_{X_i}(x)$. The performance function is then deterministically evaluated based on the generated sample set $\hat{\boldsymbol{x}} = [\hat{x}_1, \hat{x}_2, \ldots, \hat{x}_n]$ for limit state violation. If a violation occurs, the corresponding MCS trial is counted as failed. For a complete MCS, several trials N with individual sample sets $\hat{\boldsymbol{x}}_{\boldsymbol{i}}$, where $1 \leq i \leq N$, are computed. The domain of each random variable which is covered by the selected samples through all MCS trials, is thereby denoted as sampling space. Based on the total number of failed trials n_f, the probability of failure p_f can be estimated:

$$p_f \approx \frac{n_f}{N}. \tag{7}$$

This method is denoted as direct sampling or 'crude' Monte-Carlo. As already mentioned, it is the most simple MCS approach, but also not very efficient [6]. More precise results with a smaller number of samples can be achieved by the application of variance reduction methods, e.g. through stratified sampling or importance sampling schemes. However, since these methods are quite sophisticated, only crude MCS is implemented within this investigation.

2.3. Gaussian Process Regression

The Gaussian process regression (GPR) can be used to make predictions based on available observations with the advantage, that also the associated uncertainty is available as probabilistic output [8]. For this, the available observations are supposed to possess input x_i and output values y_i which are assumed to be connected through an unknown function f which is disturbed by some additive noise η [9].

$$y_i = f(x_i) + \eta_i \tag{8}$$

This unknown function f, which identification is of significant importance to perform the intended regression, can be of more or less arbitrary shape, meaning that there is an indefinite number of possible functions which could adequately describe the observations. Because of that, the GP is not representing the unknown functions themselves, it is describing their probability distribution. This means, that the corresponding probability density function of the multivariate distribution within the GP, is leading to probabilities of functions, and not scalars. This is utilized to obtain the actual regression function by computing its expected value, which is again a function. To get a better understanding of how GPR works the probability theory is considered. There, GPR is assigned to the class of Bayesian non-parametric regression models which utilizes, as indicated by its name, a Gaussian process (GP) [9]. Bayesian methods are usually characterized by defining a prior distribution based on a random function (stochastic process) which is then updated by incorporating m observations $\boldsymbol{x} = (x_1, x_2, \ \ldots \ , x_m)$ in order to generate a fitted posterior distribution [10]. When implementing a GP, these prior and posterior distributions are assumed to be normally distributed. A GP is generally defined by a mean function $\mu(\boldsymbol{x})$ and a covariance kernel function $\kappa(x_i, x_j)$. The kernel function maps covariances between each individual observation location based on their relative position in space (or time) leading to the covariance matrix $\boldsymbol{K}(\boldsymbol{x}, \boldsymbol{x})$.

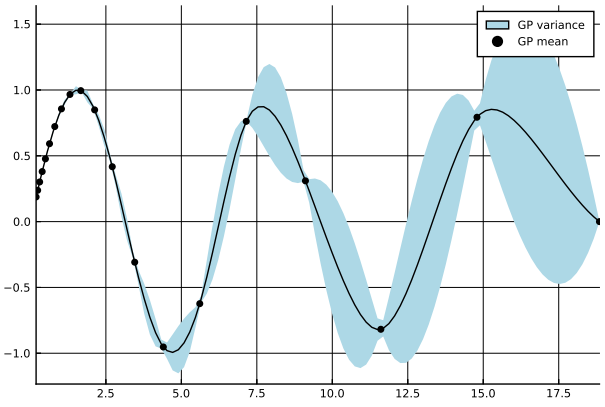

Figure 1: GPR example for $f(x) = \sin(x)$ with applied SE kernel and $l = 1$. (Prediction = solid line, variance = blue area)

$$\boldsymbol{K}(\boldsymbol{x}, \boldsymbol{x}) = \begin{pmatrix} \kappa(x_1, x_1) & \kappa(x_1, x_2) & \ldots & \kappa(x_1, x_m) \\ \kappa(x_2, x_1) & \kappa(x_2, x_2) & \ldots & \kappa(x_2, x_m) \\ \vdots & \vdots & \ddots & \vdots \\ \kappa(x_m, x_1) & \kappa(x_m, x_2) & \ldots & \kappa(x_m, x_m) \end{pmatrix}$$

The mapping depends highly on the selected kernel function as it can be demonstrated by reference to a squared exponential (SE) covariance function with a characteristic length-scale parameter l and a distance r_{ij} between two observations x_i and x_j [11]:

$$\kappa(x_i, x_j) = \exp\left(-\frac{r_{ij}^2}{2l^2}\right). \tag{9}$$

It is apparent that observations located close to each other (r_{ij} tends to 0) will result in a high covariance, whereas locations with higher relative distances (large r_{ij}) will result in low covariances. With the covariance matrix $\boldsymbol{K}(\boldsymbol{x}, \boldsymbol{x})$ the probability of the multivariate Gaussian

distribution is completely defined

$$p(\boldsymbol{y}(\boldsymbol{x})) = \mathcal{N}\left(\mu(\boldsymbol{x}), \boldsymbol{K}\left(\boldsymbol{x}, \boldsymbol{x}\right)\right) \tag{10}$$

where $\boldsymbol{x}$ and $\boldsymbol{y}$ are the observation location and result vectors. To implement a prediction or regression for an unknown location (x_*, y_*), the covariance matrix is extended within the GP [9].

$$p\left(\begin{bmatrix} \boldsymbol{y}(\boldsymbol{x}) \\ y_*(x_*) \end{bmatrix}\right) = \mathcal{N}\left(\begin{bmatrix} \mu(\boldsymbol{x}) \\ \mu(x_*) \end{bmatrix}, \begin{bmatrix} \boldsymbol{K}\left(\boldsymbol{x}, \boldsymbol{x}\right) & \boldsymbol{K}\left(\boldsymbol{x}, x_*\right) \\ \boldsymbol{K}\left(x_*, \boldsymbol{x}\right) & \kappa\left(x_*, x_*\right) \end{bmatrix}\right) \tag{11}$$

All additional parameters $\mu(x_*)$, $\boldsymbol{K}\left(\boldsymbol{x}, x_*\right)$, $\boldsymbol{K}\left(x_*, \boldsymbol{x}\right)$ and $\kappa\left(x_*, x_*\right)$ are obtainable through the already provided mean and kernel functions. To finalize the prediction, solely the univariate marginal distribution for x_*, designated as posterior distribution, must be computed from the extended GP multivariate distribution in Equation 11. From this distribution, which is Gaussian as well, the mean and variance can be obtained with basic statistics. The mean value then corresponds to the intended prediction based on the initial observations. An example of a GPR result is shown in Figure 1. There, the regression of a simple sinusoidal curve is plotted for three periods for logarithmically distributed observations. It is noticeable, that the variance raises with increasing distance between the observations, which results in a decline of the prediction accuracy. For further details on GPR, like the mathematical background or adequate kernel selection strategies, the reader is referred to the relevant literature ([8],[9],[10]).

2.4. Fatigue evaluation with uncertainties

During the verification of a wind turbine design or a structure in general, several different limit states must be considered. A limit state defines a condition where design requirements are no longer met by the considered structure or component [12]. Usually, the governing limit states are the ultimate limit states (ULS) corresponding to extreme environmental loads and the fatigue limit states (FLS) related to failure by cyclic loading [13]. When evaluating fatigue limit states, the Palmgren-Miner linear damage hypothesis [14] is used, where a linear accumulation of all experienced damages of a structure or component under consideration is applied in order to estimate the total damage. This total damage is often referred as the Miner sum and can be calculated as follows:

$$D = \sum_{i=1}^{k} \frac{n_i}{N_i} \tag{12}$$

where

D	=	accumulated fatigue damage
k	=	number of different stress ranges
n_i	=	number of stress cycles experiences at $\Delta\sigma_i$
N_i	=	number of stress cycles to failure at $\Delta\sigma_i$
$\Delta\sigma_i$	=	stress range

A violation of the fatigue limit state occurs when the accumulated fatigue damage D reaches a critical value D_{cr}. Within deterministic design, this value is normally set to be 1.0. For reliability analysis, the JCSS suggests to model D_{cr} as a lognormal distributed random variable with a mean of $\mu_{D_{cr}} = 1.0$ and a coefficient of variation of $\mathrm{CoV}_{D_{cr}} = 0.3$, since the critical damage value possesses a distinct random nature [3]. To determine the Miner sum, detailed information is required about the number of stress cycles to failure for each stress range $\Delta\sigma_i$. These are obtained in standardized fatigue tests [15], where predefined specimens are loaded periodically at constant load amplitudes until failure occurs. This is repeated several times to obtain a statistical distribution of the cycles to failure. Followed by a statistical evaluation [16], the S-N,

or Wöhler curve is obtained from the test results, which describes the finite life of a material by just two parameters as shown below:

$$\log_{10} N = \log_{10} a - m \log_{10} \Delta\sigma \tag{13}$$

where

m	=	inverse slope of the S-N curve
$\log_{10} a$	=	intercept of the log N axis
N	=	number of stress cycles to failure at $\Delta\sigma$

Typical values can be found in structural design standards. Since these are usually intended for deterministic design, a safety margin is already implemented, meaning the provided S-N data describes a quantile curve rather than the mean curve. The S-N data used within this investigation is obtained from a DNV GL Offshore Standard, which provides S-N curves as mean-minus-two-standard-deviation curves corresponding to a probability of survival of 97.7% or to a 0.023-quantile curve [17]. For usage in structural reliability, the obtained S-N data must be converted to mean-curves with probabilities of survival of 50% by adding two standard deviations σ.

$$\log_{10} N|_{50\%} = \log_{10} a|_{97.7\%} + 2\sigma - m \log_{10} \Delta\sigma \tag{14}$$

The slopes of the S-N curves remain unchanged. DNV GL defines a 'lump' standard deviation for $\log N$ of $\sigma = 0.2$ for all its S-N data, regardless which detail category is chosen for nominal stress S-N curves or whether a hot-spot stress S-N curve is used. This implies that the coefficient of variation will be different for each S-N curve. The experienced stress cycles n_i are calculated based on classical structural mechanics with time dependent load functions as inputs. For wind turbines, this is typically done by the aid of time domain analyses resulting in time dependent stress results. These are then analyzed with counting and classification methods, e.g. through the rainflow counting method [18] as used within this investigation, to separate the time depending stress signals into discrete stress cycles. These can then be evaluated according to Palmgren-Miner, as stated in Equation 12.

2.5. Numerical Wind Turbine Model

For this investigation the NREL 5-MW reference wind turbine [19] is used, together with the monopile design from the Offshore Code Comparison (OC3) project [20]. The connection to the sea bottom is defined as fixed clamping, meaning no soil model is implemented. The environmental conditions are selected from the UpWind project's K13 shallow water site [21]. As simulation environment the multi-physics simulator OpenFAST (v2.3.0) is used, which allows to perform transient analyses of the wind turbine. The wind turbine properties and site conditions are listed in Table 1. As governing load case for the fatigue design the power production design load case DLC 1.2 based on the IEC-3 Standard is utilized [22]. Within the DLC 1.2 a normal turbulence model, a normal sea state and no currents are applied. Wind and wave directions have to be considered both in-line and misaligned. The fatigue load cases have been derived from the scatter diagrams provided within the UpWind design basis for the shallow water site [21]. In total, to perform a single fatigue verification, an analysis of 43,179 different load cases is required. To reduce this number, two general measures are considered: For one, the symmetric behaviour of the monopile support structure is utilized. Only seven basic combinations of wind and wave directions are calculated for each possible configuration of wind speed, significant wave height and peak period. From these basic load cases, all possible 144 configurations within the directional scatter diagram are derived through rotation and/or mirroring of the results. By this, the number of load cases is reduced to 2,632. Further, an approach described by Stieng and Muskulus [23] is employed, where the observation is made, that for similar designs, the damage occurring in some load cases, can be predicted by the knowledge of the damage of a few load cases.

And that naturally, those load cases are selected, which generate the most partial damage. This allows for a massive reduction in number of load cases to compute. Therefore, after an initial calculation of the complete load case set, the approach leads to an additional reduction to 2,951 load cases from which only 168 are simulated based on the symmetry utilization, as described above. During verification the guidelines [12] and recommended practice for fatigue design [17] from DNV GL have been followed. Thereby we consider stress concentration factors which are used together with the hot spot S-N curve for tubular joints in seawater with cathodic protection. For evaluation, the already mentioned rainflow method is implemented with application of 270 different stress bins. The widths of the bins vary depended on the stress range magnitude. For small stress ranges up to 30 MPa, the bin widths are 0.25 MPa. For intermediate stress ranges up to 60 MPa and for large stress ranges up to 150 MPa, the widths are 0.5 MPa and 1.0 MPa, respectively. The simulation time for each load case is set to 150 seconds from which only the last 120 seconds are employed for the damage accumulation. This is a distinction from the 6×10 Minute requirement defined in the IEC-3 standard [22]. However, since this is a comparative study of different fatigue evaluation methods which are always applied to the same set of analysis results, the influence of this reduced simulation time is assessed as tolerable.

Table 1: Basic data used for model

NREL 5-MW Baseline Wind Turbine	
Rotor configuration	Upwind, 3 blades
Drivetrain, gearbox	High speed, multiple-stage
Rotor, hub diameter	126 m, 3m
Hub height	90 m
Cut-in, rated, cut-out wind	3 m/s, 11.4 m/s, 25 m/s
Cut-in, rated rotor speed	6.9 rpm, 12.1 rpm
OC3 Monopile	
Monopile diameter	6 m
Wall thickness	60 mm
Considered length	30 m
UpWind shallow water site	
Water depth	21.4 m MSL
Current normal, extreme	0.6 m/s, 1.2m/s
Weibull parameters wind	A=10.61 m/s, k=2.08 m/s
Design lifetime	20 years

2.6. Simulation approach

In order to make a comparison of the different approaches for considering uncertainties during fatigue evaluation, a Monte Carlo simulation is performed with the computation sequence as shown in Figure 2. To reduce the computation time during the MC simulation, a GPR model is implemented covering for all random variables which are directly influencing and changing the wind turbine structure. The GPR predicts the structural response with regard to the defined random input variables. During the MC simulation, the time consuming transient analyses, which would have been executed for every MC trial, are replaced by evaluations of the much faster GPR model. This reduces the total simulation time by a substantial amount.

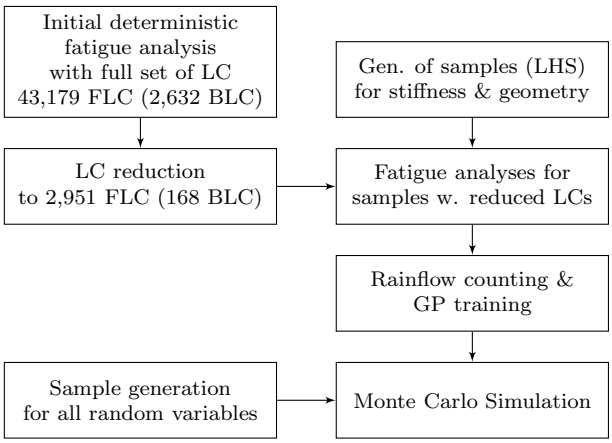

Figure 2: Calculation approach (LC = load cases; BLC = basic load cases; FLC = fatigue load cases; LHS = latin hypercube sampling).

2.6.1. Random variables The utilized random variables with their corresponding probability distributions are summarized in Table 2. The random variables for stiffness $\boldsymbol{K}$ and geometry $\boldsymbol{G}$, with mean values of 1.0 each, are relative measures. This definition is based on the implementation possibilities within the simulation environment OpenFAST. Here, the wind

turbine's support structure and tower structure are considered in separate sub-modules with different modelling approaches. The substructure geometry is implemented through direct input of the dimensions of the elements and assigned to a linear elastic and isotropic material with underlying information for the Young's modulus E. In this case, where a monopile structure is used, the geometry inputs correspond to the outer diameters D_i and the thicknesses of the tubular sections t_i. For generating sample diameters $\hat{D}_i$ and sample thicknesses $\hat{t}_i$, their nominal values are multiplied with the sample geometry value $\hat{G}_i$. For generating sample values for the Young's modulus $\hat{E}_i$, their nominal values are multiplied with the sample stiffness value $\hat{K}_i$. The tower geometry is implemented within OpenFAST only in terms of distributed stiffnesses K_d over the tower length. Therefore, only a dependency on the random variable $\boldsymbol{K}$ is implemented for the tower. Sample values for the distributed stiffnesses $\hat{K}_{d_i}$ are produced by multiplication of their nominal values with the sample stiffness value $\hat{K}_i$. To consider the random variable $\boldsymbol{S}$ for the S-N curve data, the mean S-N curve μ_S must be obtained.

$$\log_{10} N|_{50\%} = \underbrace{\log_{10} a|_{97.7\%} + 2\sigma_S}_{\mu_S} - m \log_{10} \Delta\sigma \tag{15}$$

Here, the hot spot stress S-N curve for tubular joints in seawater with cathodic protection is considered, the intercept of the log N axis for the steeper curve part is given by $\log_{10} a = 10.18$ [17]. With the standard deviation of $\sigma_S = 0.2$, a mean value of $\mu_S = 10.58$ follows. The distribution of $\boldsymbol{S}$ is thus $\mathcal{N}(\mu_S, \sigma_S)$ or respectively $\mathcal{N}(10.58, 0.2)$. Given a sample $\hat{S}$, the following effective S-N curve is then used:

$$\log_{10} N = \hat{S} - m \log_{10} \Delta\sigma. \tag{16}$$

Table 2: Overview of random variables.

	Parameter	Distribution	Mean μ	CoV
$\boldsymbol{K}$	Stiffness	lognormal	1.0	0.005
$\boldsymbol{G}$	Geometry	lognormal	1.0	0.010
$\boldsymbol{D}_{cr}$	Miner sum	lognormal	1.0	0.300
$\boldsymbol{S}$	S-N data	normal	–	$\sigma = 0.2$

Table 3: Overview of implemented GPRs.

Item	Amount
Evaluated nodes along the MP height	13
Circumferential evaluation points	60
Stress bins per evaluation point	270
Number of GPR models	210, 600

2.6.2. Gaussian Process Regression To replace the transient structural simulation with the evaluation of a GPR model, the required outputs must be identified. For that, the Miner sum from Equation 12 is considered once again. Here, the partial fatigue damage D_i is calculated through dividing the experienced stress cycles n_i for a given stress range $\Delta\sigma_i$ by the number of stress cycles leading to structural failure N_i at the same stress range. To obtain the total damage D, the partial damages are accumulated over all stress ranges. This time, the Miner sum is expressed as a LSF:

$$G(R - S) = D_{cr} - \sum_{i=1}^{k} \frac{n_i}{N_i} \leq 0. \tag{17}$$

As already partly indicated, the resistances, namely the stress cycles leading to structural failure N and the critical Miner sum D_{cr}, are both post-processing variables which are not involved in the actual structural simulations. Only the number n of stress cycles experienced (for each stress rang considered) are actual outputs from the time consuming simulations. Therefore, these are modeled by a Gaussian Process. To implement this, training data is needed which must be

dependent to the two basic random variables for stiffness $\boldsymbol{K}$ and geometry $\boldsymbol{G}$. This is obtained by sampling from both variables. Subsequently, the OpenFAST inputs are adjusted for each sample of scaling factors (see above) and used to perform the structural simulations in order to obtain the experienced stress cycles. For the training of the model an optimised Latin Hypercube Sampling (LHS) approach is implemented based on the work of Bates [24]. In total $n_{LHS} = 50$ training sets are produced and used for the simulations. In order to better fit the tail behavior of the random variables, the region for which LHS is applied, is slightly increased. Therefor, the CoV values of the random variables are raised by 25%, each. The time-dependent stress results, obtained at several different evaluation positions along the monopile (MP), are transformed into stress cycles which are allocated into different stress range bins through the rainflow counting approach as stated earlier. The obtained number n_{sim} of cycles within the simulation time t_{sim} are proportionally increased to match the number of cycles n_{tot} during the complete turbine's design life t_{tot}.

$$n_{tot} = \frac{t_{tot}}{t_{sim}} \cdot P_{LC} \cdot n_{sim} \tag{18}$$

The increases are based on the provided load case probabilities of occurrence P_{LC} as given in the scatter diagrams of the UpWind design basis [21]. The total number of cycles per stress range bin is obtained by summing this over all load cases. This procedure is repeated for all samples according to the LHS approach, leading to training data consisting of stress cycle information for each stress range bin obtained at different realizations for $\boldsymbol{K}$ and $\boldsymbol{G}$. Based on this training data, GPR are implemented for each of the 270 stress range bins. By this a single GPR model approximates the number of stress cycles for a given sample set $\left(\hat{K}, \hat{G}\right)$. To obtain the complete structural response, the GPR models of every bin must be executed. The GPR is implemented through the Julia library from Fairbrother et. al [25]. As covariance function a standard Matérn class kernel with $\nu = 3/2$ is considered based on previous works of Stieng and Muskulus [26]. The length-scale parameter is thereby set to $l = 1.0$. An overview of the number of GPR models is given in Table 3.

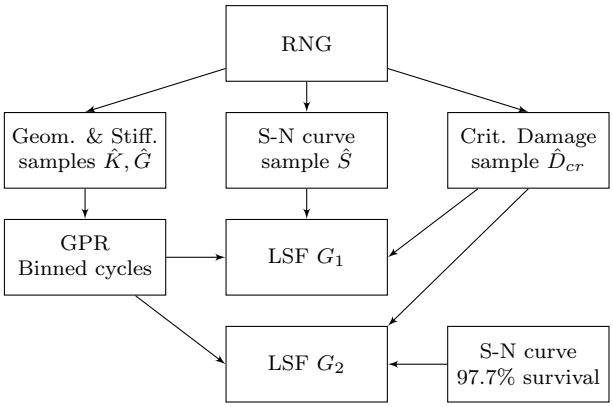

Figure 3: Implemented MC procedure with parallel utilization of sampled data.

2.6.3. Monte Carlo Simulation In order to implement the MC simulation process, four fatigue LSF are defined, which are all based on Equation 17. Fatigue LSF G_1 considers all introduced random variables $\boldsymbol{K}, \boldsymbol{G}, \boldsymbol{D}_{cr}$ and $\boldsymbol{S}$:

$$G_1(\boldsymbol{K}, \boldsymbol{G}, \boldsymbol{D}_{cr}, \boldsymbol{S}) = \boldsymbol{D}_{cr} - \sum_{i=1}^{k} \frac{n_i(\boldsymbol{K}, \boldsymbol{G})}{N_i(\boldsymbol{S})}. \tag{19}$$

The other fatigue LSF are defined analogously, but their dependence on the random variables differs. The random variables $\boldsymbol{K}$ and $\boldsymbol{G}$ are always taken into account, but the consideration of $\boldsymbol{D}_{cr}$ and $\boldsymbol{S}$ is different for each LSF. G_2 utilizes an uncertain critical Miner sum threshold $\boldsymbol{D}_{cr}$, but a deterministic S-N curve with 97.7% of survival. Fatigue LSF G_3 is purely deterministic, with a critical Miner sum threshold of $D_{cr} = 1$, and the 97.7% S-N curve. Fatigue LSF G_4 has a critical Miner sum threshold of $D_{cr} = 1$, but an uncertain S-N curve. The procedure to evaluate a

single MC sample is illustrated in Figure 3 for the two major FLS G_1 and G_2. As shown, random numbers are generated for each of the random variables according to their defined probability distributions. As random number generator (RNG) a Mersenne Twister is used [27]. To obtain properly distributed random numbers the inverse transform method is utilized [6]. The two samples $\hat{K}$ and $\hat{G}$ are used within the GPR as described in the previous subsection to obtain the binned stress cycles. With $\hat{S}$ the effective S-N curve is determined. Finally, with consideration of $\hat{D}_{cr}$ the LSF G_1 is evaluated. For evaluating LSF G_2, a deterministic S-N curve is utilized. The process for LSF G_3 and G_4 is similar. To reduce the computation time all LSF evaluations are based on the same sample sets, meaning that the generated stress cycle bin information, the critical damage values, and the S-N curve data are re-used. Finally, the MC simulation trials are checked for violation of every LSF in order to obtain their corresponding probabilities of failure:

$$\hat{p}_{fi} = P\left(G_i \leq 0\right) \approx \frac{n_{\text{failed}}}{N_{\text{total}}}. \tag{20}$$

The accuracy of these estimators $\hat{p}_{fi}$, which is highly dependent on the number of total samples N_{total}, can be expressed through their coefficients of variation (CoV) [28]:

$$CoV_i = \sqrt{\frac{1-\hat{p}_{fi}}{N_{total} \cdot \hat{p}_f}}. \tag{21}$$

Since it is targeted for a CoV of approximately 10% for a probability of failure with a magnitude of $\hat{p}_f = 10^{-4}$, the sampling process is repeated $n_{MC} = 1,064,000$ times.

3. Results

As final measure the reliability indices β_i are computed as described previously in Section 2.1. An overview of all results is given below.

Table 4: Summary of MC simulation results at $N_{\text{total}} = 1,064,000$ trials

Result description		LSF G_1	LSF G_2	LSF G_3	LSF G_4
$\hat{S}$	S-N Curve	Random	Deterministic	Deterministic	Random
$\hat{D}_{cr}$	Critical Miner sum	Random	Random	Deterministic	Deterministic
n_{failed}	Failed trials	221	1,696	792	96
$\hat{p}_f$	Failure probability	$2.077 \cdot 10^{-4}$	$15.940 \cdot 10^{-4}$	$7.444 \cdot 10^{-4}$	$0.649 \cdot 10^{-4}$
CoV	Coefficient of variation	6.7%	2.4%	3.5%	12.0%
β	Reliability index	3.53	2.95	3.18	3.83

During implementation of the GP, it is noted, that the amount of available training data varies for different stress ranges. For low stress ranges, cycle information are provided by every training sample. In regions of high stress ranges, less data is available, meaning only a small number, or even just single training samples, feature cycle information.

4. Discussion

4.1. Major findings

4.1.1. General outcome As noticeable from the presented results, the reliability index $\beta_1 = 3.53$ for LSF G_1, where an uncertain S-N curve is implemented, is higher compared the reliability index $\beta_2 = 2.95$ for LSF G_2, where always a S-N curve with 97.7 % of survival is utilized. This is convincing, since due to the consideration of random S-N data, 97.7 % of all samples are higher compared to the fixed S-N curve. Consequently, lower limit state violations are in place because

in nearly all cases the resistances are higher compared to LSF G_2. This can be verified by the computed data, in 1,039,738 cases the S-N curves lie above the fixed curve,which corresponds to 97.72 % and matches the expectations. By comparing the results of G_2 and G_3 it is noticeable that the influence of the uncertain critical Miner sum $\boldsymbol{D}_{cr}$ is somewhat smaller. The obtained reliability index $\beta_3 = 3.18$ for a deterministic value of $D_{cr} = 1.0$ is only slightly greater than in the uncertain case with $\beta_2 = 2.95$. This is founded in the underlying lognormal distribution of the critical Miner sum $\boldsymbol{D}_{cr}$, which possesses its maximum probability density just slightly below 1.0, leading to approximately 56% of critical Miner sum samples smaller than in the deterministic case. The highest influence on the reliability has the uncertain S-N curve as can be seen from the obtained reliability index $\beta_4 = 3.83$ for G_4. Therefore, from a design perspective, the results lead to the conclusion that by evaluating the S-N curve probabilistically, indeed a less conservative approach is employed, though the reliability changes significantly which makes an exploitation of considerable design capacities possible.

4.2. Outlook

For the comparison part of the fatigue evaluations, further investigations with prolonged simulation time might be required in order to increase the accuracy of the obtained reliability results. The simulation time incorporated within this study is small compared to the requirements of typical design standards as described in Section 2.5. Longer simulation times increase the possibility to capture extremes within the stochastic wave loading or extremes of the structural response. Due to the short simulation times, such phenomena might be not covered, which could lead to an overestimation of the obtained reliabilities. However, since the fatigue evaluations for all LS are based on the same response data, we believe, that the order of reliability increase between a deterministic and an uncertain S-N curve is still valid. From the pure analysis perspective, several items could be improved or enhanced. For one, the number of uncertainties pictured within this investigation is low, especially uncertainties in environmental conditions are currently not considered. These could be fitted to a Weibull distribution with random parameters. Likewise, further uncertainties could be added to the wind turbine model, such as uncertainties within the soil behavior and the related stiffness of the bottom support. These have been left out since it is not feasible to implement spring elements within the OpenFAST environment without rewriting and recompiling the source code. In further investigations the pile could be extended and horizontally supported to match the lateral soil stiffness. The model approach could be adjusted as well. The sparsely populated stress cycle bins at high stress ranges might be further investigated in detail to determine their influence towards the accuracy of the GPR. The same applies to the selection of the GPR kernel and the settings of the corresponding kernel parameters.

4.3. Conclusion

The influence of different uncertainties within the Palmgren-Miner linear damage hypothesis on the structural reliability has been examined. For this, reliability analyses for the fatigue limit state of an offshore wind turbine monopile support structure have been conducted. Different configurations with deterministic and uncertain values for the S-N curve and for the critical Miner sum D_{cr} have been analyzed by implementing a crude Monte Carlo approach. To reduce the computational effort, surrogate models, which are based on Gaussian Processes Regression, and trained by several numerical simulations, have been used. These approximate the required structural responses within the crude Monte Carlo simulations, and in this way, allow for the computation of the structural reliability in a manageable time. The results show that an uncertain S-N curve substantially influences the reliability. Compared to a complete deterministic configuration, where the S-N curve and the critical Miner sum are selected as specified by governing design standards, the reliability index significantly increases from $\beta_3 = 3.18$ to

$\beta_4 = 3.83$. On the contrary, the impact of an uncertain critical Miner sum is marginal and even leads to a lower reliability. In comparison to the complete deterministic configuration, the reliability index is slightly reduced from $\beta_3 = 3.18$ to $\beta_2 = 2.95$. This corresponds to the findings of Dragt et. al. [29], where the influence of load sequence effects through over- and underloads together with mean changes were studied, and more advanced fracture mechanics methods were applied. Their results show, that under realistic loading conditions for wind turbines, sequence effects only have a minor impact on the fatigue life. Consequently, for a configuration with both uncertainties in the Palmgren-Miner linear damage hypothesis, the obtained reliability index $\beta_1 = 3.53$ is higher than in the deterministic case and shows the prevalent influence of the uncertain S-N curve.

References

[1] DNV GL 2019 *Energy Transition Outlook 2019 - Power Supply and Use.* (Høvik: DNV GL AS)
[2] Sørensen J D and Toft H S 2010 *Energies* **3** 241–257
[3] Joint Commitee On Structural Safety J 2011 *Probabilistic Model Code Part 3: Resistance Models* (JCSS)
[4] Thoft-Christensen P and Murotsu Y 1986 *Application of Structural Systems Reliability Theory* (Berlin: Springer)
[5] Hu C, Youn B D and Wang P 2019 *Engineering Design under Uncertainty and Health Prognostics* (Cham: Springer)
[6] Melchers R E and Beck A T 2018 *Structural Reliability Analysis and Prediction* (Hoboken: Wiley)
[7] Zio E 2013 *The Monte Carlo Simulation Method for System Reliability and Risk Analysis* (London: Springer)
[8] Murphy K P 2012 *Machine Learning: A Probabilistic Perspective* (Cambridge: MIT Press)
[9] Roberts S, Osborne M, Ebden M, Reece S, Gibson N and Aigrain S 2013 *Phil. Trans. R. Soc. A.* **371** 20110550
[10] Gelman A, Carlin J B, Stern H S, Dunson D B, Vehtari A and Rubin D B 2013 *Bayesian Data Analysis* (Boca Raton: CRC Press)
[11] Rasmussen C E and Williams C K I 2006 *Gaussian Processes for Machine Learning* (Cambridge: MIT Press)
[12] DNV GL 2016 *Standard DNVGL-ST-0126 - Support Structures for Wind Turbines.* (Høvik: DNV GL AS)
[13] DNV GL 2019 *Offshore Standard DNVGL-OS-C101 - Design of Offshore Steel Structures, General - LRFD Method.* (Høvik: DNV GL AS)
[14] Miner M 1945 *Journal of Applied Mechanics* **12** A159–A164
[15] DIN *DIN 50100:2016-12, Load Controlled Fatigue Testing - Execution and Evaluation of Cyclic Tests at Constant Load Amplitudes on Metallic Specimens and Components* (Berlin: Beuth)
[16] Masendorf R and Müller C 2018 *Material Testing* **60** 961–968
[17] DNV GL 2016 *Recommended Practice DNVGL-RP-C203 - Fatigue Design of Offshore Steel Structures.* (Høvik: DNV GL AS)
[18] Rychlik I 1987 *International Journal of Fatigue* **9** 119–121
[19] Jonkman J, Butterfield S, Musial W and Scott G 2009 *Definition of a 5MW Reference Wind Turbine for Offshore System Development* (Golden: NREL)
[20] Vorpahl F, Strobel M, Jonkman J, Larsen T and Passon P 2014 *Wind Energy* **17** 519–547
[21] Fischer T, de Vries and Schmidt B 2010 *Upwind Design Basis - WP4: Offshore Foundations and Support Structures* (Stuttgart: UpWind)
[22] International Electrotechnical Commission 2019 *IEC 61400-3-1:2019, Wind Energy Generation Systems Part 3-1: Design Requirements for Fixed Offshore Wind Turbines.* (Geneva: IEC)
[23] Stieng L E S and Muskulus M 2018 *Wind Energy Science* **3** 805–818
[24] Bates S, Sienz J and Toropov V 2004 *Proc. 45th AIAA/ASME/ASCE/AHS/ASC Structures, Structural Dynamics & Materials Conf. (Palm-Springs)*
[25] Fairbrother J, Nemeth C, Rischard M, Brea J and Pinder T 2019 *arXiv* 1812.09064
[26] Stieng L E S and Muskulus M 2020 *Wind Energy Science* **5** 171–198
[27] Matsumoto M and Nishimura T 1998 *ACM Trans. Model. Comput. Simul.* **8** 3–30
[28] Menz M, Dubreuil S, Morio J, Gogu C, Bartoli N and Chiron M 2020 *arXiv* 2011.15001
[29] Dragt R C, Hengeveld S T and Maljaars J 2018 *Proc. 28th Int. Ocean and Polar Engineering Conf. (Sapporo)* pp 265–272